

CALVERA: A LOW-MASS STRANGEON STAR TORQUED BY DEBRIS DISK?

YUNYANG LI

School of Physics and State Key Laboratory of Nuclear Physics and Technology, Peking University, Beijing 100871, China

WEIYANG WANG

School of Physics and State Key Laboratory of Nuclear Physics and Technology, Peking University, Beijing 100871, China

Key Laboratory of Computational Astrophysics, National Astronomical Observatories, CAS, Beijing 100012, China
and

School of Astronomy and Space Sciences, University of Chinese Academy of Sciences, Beijing 100049, China

MINGYU GE

Key Laboratory for Particle Astrophysics, Institute of High Energy Physics, Chinese Academy of Sciences, Beijing 100049, China

XIONGWEI LIU

School of Physics and Space Science, China West Normal University, Nanchong 637002, China

HAO TONG

School of Physics and Electronic Engineering, Guangzhou University, Guangzhou 510006, China

RENXIN XU

School of Physics and State Key Laboratory of Nuclear Physics and Technology, Peking University, Beijing 100871, China
and

Kavli Institute for Astronomy and Astrophysics, Peking University, Beijing 100871, China

(Received Sep 19, 2017; Revised XXXX; Accepted XXXX)

ABSTRACT

Calvera is a 59 ms isolated pulsar, being unique due to its non-detection in radio, optical and gamma-rays but the purely thermal emission in soft X-rays. It is suggested that Calvera could be an ordinary middle-aged pulsar with significant magnetospheric activity at a large distance (Shibanov et al. 2016). Alternatively, it is proposed in this paper that Calvera is a low-mass strangeon star with inactive magnetosphere (dead). In this scenario, we jointly fit the spectra obtained by the *XMM-Newton* Observatory and the *Chandra* X-ray Observatory with the strangeon star atmosphere model. The spectral model is successful in explaining the radiation properties of Calvera and X-ray Dim Isolated Neutron Stars, both showing similar observation features. Within the dead pulsar picture, Calvera might be of high temperature at 0.67 keV, possessing a small magnetic field $B \lesssim 10^{11}$ G and a small stellar radius $R \lesssim 4$ km and is probably braked by the fall-back disk accretion. Future advanced facilities may provide unique opportunities to know the real nature of Calvera.

Keywords: pulsars: individual (Calvera, 1RXS J141256.0+792204) – stars:neutron – accretion

1. INTRODUCTION

The *ROSAT* All-Sky Survey discovered a high galactic latitude ($b = 37^\circ$) compact object, 1RXS J141256.0+792204 (Rutledge et al. 2008), which was then identified as an isolated neutron star (INS, hereafter “NS” refers to all kinds of pulsar-like compact objects) candidate. The fact that this INS is discovered after the seven radio-quiet and thermally emitting X-ray dim isolated neutron star (XDINS), the Magnificent Seven (see Haberl 2007; Kaplan 2008, for reviews), leads it to be nicknamed as “Calvera”. Calvera, in particular, is a puzzling source that has some confusion in the classification among the neutron star family.

Calvera exhibits X-ray pulsations with period $P = 59$ ms (Zane et al. 2011) and spin-down rate $\dot{P} = 3.2 \times 10^{-15} \text{ s s}^{-1}$ (Halpern et al. 2013; Halpern & Gotthelf 2015), making its location in the $P - \dot{P}$ diagram (Figure 1) far from the Magnificent Seven class, which are slowly rotating ($P \sim 3 - 11$ s) NSs. It is also speculated that Calvera might be a candidate of the central compact object (CCO, Rutledge et al. 2008; Zane et al. 2011; Gotthelf et al. 2013). However, Calvera presents a larger dipole magnetic field (Shevchuk et al. 2009) and there is still no conclusive evidence for the host supernova remnant (Zane et al. 2011). Alternatively, there are suggestions that the magnetic field ($\sim 10^{12}$ G) of CCO is buried by prompt fall-back of a small amount of supernova ejecta (Ho 2011; Viganò & Pons 2012; Bernal et al. 2013); therefore, Calvera could be a descendant of the CCO reemerging the magnetic field (Halpern et al. 2013).

It is odd that deep search failed to detect the radio emission from this source (Hessels et al. 2007; Zane et al. 2011). The non-detection of radio emission from Calvera can not be simply attributed to the unfavored beaming effect since emission features are nor found in gamma-rays (Halpern 2011; Halpern et al. 2013) which commonly correspond to a larger beaming angle. This can be explained by a distant location of Calvera (e.g., 1.5 – 5 kpc, Shibano et al. 2016), but that would place it high above the Galactic disk and cause problem for its birth place, given its rather small proper motion ($69 \pm 26 \text{ mas yr}^{-1}$, Halpern & Gotthelf 2015). Moreover, attempts also failed in searching for non-thermal emission feature in the soft X-ray band (Zane et al. 2011; Halpern et al. 2013). All these observational facts could contain hints for an inactive-magnetosphere (i.e., dead) scenario which will be discussed in this work.

The dead-pulsar-scenario is hardly understood in the framework of NS due to its high position above the NS death line (Figure 1). Spectral fits for Calvera with neutron star atmosphere model result

in small emission-radius-to-distance ratio, which forces Shibano et al. (2016) to conclude a large distance. Alternatively, we explore the possibility that Calvera is a small radius strangeon star. “Strangeon” (Lai & Xu 2017), previously known as “strange quark-cluster” (Xu 2003) is a prospective candidate for the pulsar constituent and have been successfully applied to solve problems including glitches (Zhou et al. 2014); high mass NS (Lai & Xu 2009, 2011); ultra low-mass and small radius NS (Li et al. 2015). A radiative model of the strangeon star atmosphere (SSA, Wang et al. 2017b,a) is also developed to solve the optical/ultraviolet(UV) excess problem (Walter & Matthews 1997; van Kerkwijk & Kulkarni 2001; Kaplan et al. 2011) and the Rayleigh-Jeans deviation problem (Kaplan et al. 2011) of XDINSs. The luminosity of strangeon star is maintained by accretion (Wang et al. 2017b) that would also exert a braking torque accounting for the spin-down rate. It is proposed here that Calvera is a low-mass strangeon star with an inactive magnetosphere and probably braked by the accretion flow. In this picture, Calvera and XDINSs, having similar radiative properties, can be understood as strangeon stars at different stages of the evolution.

We introduce the data reduction procedure and spectra modeling in Section 2 and ??, respectively. In Section 4 we constrain the parameters of Calvera as an isolated dead-pulsar while in Section 5 we re-consider this issue by taking into account the accretion effects. We discuss the nature of Calvera in Section 6. Summary and future possible observations in constraining the nature of Calvera are presented in Section 7.

2. DATA REDUCTION

Since the first detection by *ROSAT* (Voges et al. 1999), X-ray observations on Calvera have been made several times by *Swift* (Rutledge et al. 2008), *XMM-Newton* (Zane et al. 2011) and *Chandra* (Shevchuk et al. 2009; Halpern et al. 2013; Halpern & Gotthelf 2015). Despite numerous attempts in modeling the X-ray spectra, the nature of Calvera still remains open. In this work, we make a joint analysis (also see, Shibano et al. 2016) for the spectral data obtained by *XMM-Newton* and *Chandra* to further investigate the properties of Calvera. *Swift* data are omitted due to its limited counting statistics (Rutledge et al. 2008).

2.1. *Chandra*

We retrieved the *Chandra* Advanced Camera for Imaging and Spectroscopy (ACIS) data from the public archive. Among which, one (obs.ID 9141, Shevchuk et al. 2009) operated in the VFAINT mode and two (obs.ID 13788,15613, Halpern et al. 2013) in the continuous-clocking (CC) mode. The data re-

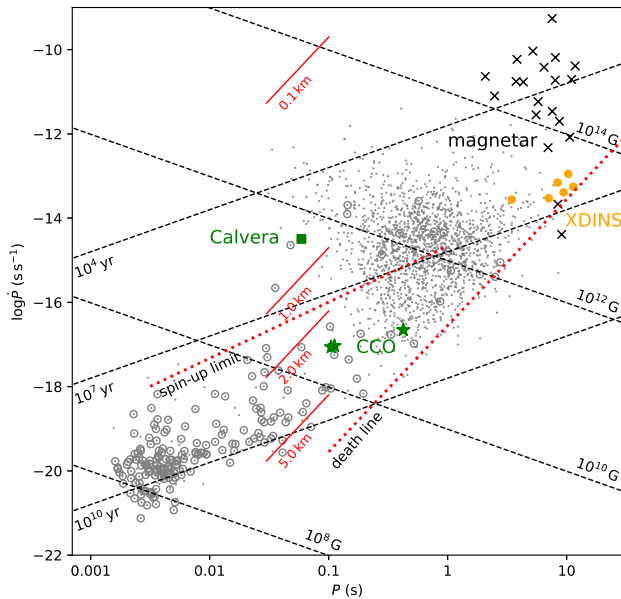


Figure 1. The $P - \dot{P}$ diagram for radio pulsars (gray dots), binary pulsars (circlets), magnetars (crosses), XDINSs (orange dots), CCOs (green stars) and Calvera (green square). The pulsar population data are from *ATNF Pulsar Catalogue* (Manchester et al. 2005). The spin data of the three CCOs are from Halpern & Gotthelf (2010) and Gotthelf et al. (2013). The spin-up limit is shown as the upper red dotted line ($P = 1.9 (B/10^9 \text{ G})^{6/7} \text{ ms}$, van den Heuvel 1987). The death line for a typical $R = 10 \text{ km}$ neutron star is indicated by the lower red dotted line ($BP^{-2} = 1.7 \times 10^{11} \text{ G s}^{-2}$, Bhattacharya et al. 1992). The death lines for low-mass strangeon star with two times the nuclear density and different stellar radii are denoted as red solid lines, on the assumption that a pulsar is torqued by magnetospheric activity.

duction and analysis were performed with the *Chandra* Interactive Analysis of Observation (CIAO, version 4.9, Fruscione et al. 2006) with calibration database (CALDB 4.7.4). For obs.ID 9141, we extracted 3599 source photons from a circle centered on the target with radius $4.16''$ and 92 background counts from the annulus surrounding the source region with an outer radius $8.32''$. For data obtained in the CC mode, source counts were extracted from a 5-column-box (15 pixels) centered on the target and the background counts from a 5-column-box away from the source. The two CC mode observations were weighed by the exposure time and combined together. All *Chandra* spectra were grouped with a minimum of 25 counts per bin. We used the *Chandra* “soft band” $0.5 - 2.0 \text{ keV}$ for modeling.

2.2. XMM-Newton

The data reduction for *XMM-Newton* were performed with Science Analysis System (SAS, version 16.0.0, SAS development Team 2014). We utilized the European Photon Imaging Camera (EPIC)-pn data of the *XMM-Newton* observations (obs.ID: 0601180101, 0601180201, Zane et al. 2011). Data from the two EPIC-MOS cameras were not used in our analysis due to its smaller effective area at soft X-ray band (Turner et al. 2001). All observations were obtained in Small Window (SW) mode with the thin filter. Good time intervals were chosen according to the light curves at $0.1 - 5 \text{ keV}$ band. The source photons were extracted from the circular region with radii $15''$ and the background from the adjacent source free region of same size. For spectral analysis, we selected single pixel events (PATTERN=0) and excluded bad CCD pixels and columns (FLAG=0). The *XMM-Newton* spectra were grouped with at least 30 counts per bin; events within the $0.1 - 3.0 \text{ keV}$ range were adopted for modeling.

The information of the data used are summarized in Table 1 for reference. All spectra modeling were performed with XSPEC version 12.9.1 (Arnaud 1996).

Table 1. Summary of the X-ray data

Data	Instrument/mode	Counts	Exposure Time (ks)	Start Date	End Date	
<i>Chandra</i>	9141	ACIS-S(VF)	3599	26.43	2008-04-08 03:42:08	2008-04-08 12:13:24
	13788	ACIS-S(CC)	2356	19.68	2013-02-12 19:28:07	2013-02-13 01:24:58
	15613	ACIS-S(CC)	2155	17.09	2013-02-18 02:52:52	2013-02-18 08:03:38
<i>XMM-Newton</i>	0601180101	EPIC-pn(SW)	8921	13.94	2009-08-31 07:07:52	2009-08-31 15:08:42
	0601180201	EPIC-pn(SW)	11411	19.48	2009-10-10 04:08:42	2009-10-10 12:26:09

3. SPECTRAL MODELING

It is suggested that pulsars could be strangeon stars (Lai & Xu 2017). A strangeon star can be thought as

a 3-flavored gigantic nucleus, and strangeons (coined by combining “strange nucleons”) are its constituent as an analogy of nucleons which are the constituent of a normal (micro) nucleus. The radiative model of the strangeon star atmosphere was put forth by (Wang et al. 2017b). For an isolated strangeon star, normal matter (i.e., composed by u, d quarks) accreted onto the stellar surface can not be converted to strangeons (i.e., strangeonization) instantly because the collision timescale $\tau_{\text{col}} \sim 10^{-22} - 10^{-20}$ s is far smaller than that of the weak interaction $\tau_{\text{weak}} \sim 10^{-7}$ s. Therefore the unconverted matter would be re-bounced and form a thermally emissive atmosphere. The flux can be described as

$$F_{\nu}^{\infty} \propto B_{\nu}(1 - e^{-2\tau_{\infty}(\nu)}), \quad (1)$$

where F_{ν} is the flux at frequency ν and B_{ν} is the blackbody spectrum. $\tau_{\infty}(\nu)$ is the observed optical depth, with the factor 2 accounting for the surface reflection (Wang et al. 2017a), and can be expressed as

$$\tau_{\infty}(\nu) = 3.92 \times 10^{-45} \frac{n_{i0}^2 (kT_i)_{\text{keV}}}{(h\nu)_{\text{keV}}^{3.5} R_{\text{km}}} (1 - e^{-\frac{h\nu}{kT_e}}), \quad (2)$$

where n_{i0} is the ion density at bottom, T_i and T_e are the ion and electron temperatures, respectively, and R is the stellar radius. We use the notation $y = n_{i0}^2 (kT_i)_{\text{keV}} / R_{\text{km}} \sim 10^{42} \text{ keV km}^{-1} \text{ cm}^{-6}$ for these degenerate parameters which is different from the one used in Wang et al. (2017b,a) by $1/R$ (the SSA model with this new definition is now uploaded to Xspec for public use). At lower energies (i.e., optical/UV bands), the optical depths are high and the radiation behaves like a blackbody. Whereas for soft X-rays, the typical optical depths are small and the flux can be approximated by $F_{\nu} = 2\tau(\nu)B_{\nu}$, which is lower than a pure blackbody spectrum. Therefore, extrapolating the blackbody spectrum obtained in the X-ray band will meet the optical/UV excess problem (Kaplan et al. 2011). The low optical depths in X-rays have two consequences: (1) Parameter y is partially degenerate with the normalization $(R_{\text{km}}/d_{10 \text{ kpc}})^2$ and the two cannot be determined simultaneously without the knowledge of the optical/UV flux. (2) Since the optical/UV excess is expected from a simple extrapolation of the blackbody spectrum in the X-rays, we can use the extrapolation of the pure blackbody fit for X-rays at optical band as a lower limit for the normalization. On the other hand, optical upper limit were obtained by *Gemini-North* (g band, Rutledge et al. 2008) and Gran Telescopio Canarias (GTC, g' , r' bands, Shibano et al. 2016), which give the upper limit of the normalization.

The phase-averaged spectral analysis was performed simultaneously for data obtained with different detec-

tors or at different times, allowing only the parameter y to vary independently to account for possible cross-calibration uncertainties. The fit was conducted with blackbody model (BB) and SSA model with fixed N_{H} (F, with N_{H} fixed to the Galactic value, Kalberla et al. 2005) or R^{∞} (M1, M2). The upper limit of the normalization (M1) was chosen such that the extrapolated spectrum meet the upper limit at GTC g' band. The lower limit (M2) was chosen such that the extrapolated spectrum converges with the blackbody fit at lower energies (e.g., \sim eV). Results are listed in Table 2 and illustrated in Figure 2.

As is shown in Shevchuk et al. (2009), Zane et al. (2011) and Halpern et al. (2013), single thermal spectra, either blackbody or pure hydrogen atmospheric model (NSA), can not provide decent fit, and two thermal components is required. The first joint fit for all available data is performed by Shibano et al. (2016), who use a single component magnetized hydrogen atmosphere model to account for the inhomogeneities of the stellar surface. Assuming a magnetic field $B = 10^{12}$ G, they obtain good fits in spite of the viewing geometry. These results are broadly consistent in the sense that $T^{\infty} \sim 200$ eV for blackbody models and $T^{\infty} \lesssim 100$ eV for NSA models and emission area $R^{\infty}/d = 2 - 4 \text{ km kpc}^{-1}$ (Rutledge et al. 2008; Shevchuk et al. 2009; Zane et al. 2011; Halpern et al. 2013; Shibano et al. 2016). In our SSA model, we obtain a higher temperature at $\gtrsim 0.6$ keV and rather unconstrained radius $R^{\infty}/d = 0.4 - 10 \text{ km kpc}^{-1}$. Zane et al. (2011) report that two-thermal models result in N_{H} larger than the Galactic value while we find that acceptable N_{H} values can be achieved assuming smaller R^{∞}/d (F and M2). The small stellar radii in the magnetized NSA model lead to the conclusion of a large distance (1.5 – 5 kpc, Shibano et al. 2016), however this is not a problem for the SSA model since strangeon star can be a few kilometers in radius.

Absorption features about 0.6 – 0.7 keV are also reported as lines (Shevchuk et al. 2009; Zane et al. 2011; Shibano et al. 2016) or edges (Zane et al. 2011). We conducted similar fitting procedure and find that absorption edges or Gaussian absorption lines equally improve the fit for model F, M1 and M2. The results for the SSA model multiplied by a *gabs* model are list in Table 2. The additional absorption line is found at 0.73 ± 0.03 keV, consistent with Shibano et al. (2016). The presence of absorption line is often attributed to the magnetic field. In this case, the absorption line might indicate $B = 6 \times 10^{10}$ G assuming electron cyclotron of neutron star, or $B = 1.2 \times 10^{11}$ G for strangeon star hydrocyclotron (Xu et al. 2012).

Table 2. Summary of spectral modeling for Calvera

Model ^a	N_{H} (10^{20} cm^{-2})	kT_e (keV)	y ($10^{42} \text{ keV km}^{-1} \text{ cm}^{-6}$)	R^∞ ($d_{\text{kpc}} \text{ km}$)	E (keV)	τ^b	EW (eV)	$F_X(0.3 - 10 \text{ keV})$ $10^{-13} \text{ erg cm}^{-2} \text{ s}^{-1}$	$\chi_\nu^2/\text{d.o.f}$
BB ^c	0	0.2	—	0.6	—	—	—	6.2	1.97/482
F	2.7	0.67 ± 0.02	5.6	0.51 ± 0.03	—	—	—	8.4	1.06/482
M1	5.0 ± 0.4	0.64 ± 0.02	0.02	10	—	—	—	10.0	1.04/482
M2	1.3 ± 0.2	0.67 ± 0.02	10.1	0.37	—	—	—	7.7	1.09/482
F	2.7	0.62 ± 0.03	7.6	$0.48^{+0.02}_{-0.01}$	0.72 ± 0.03	0.19 ± 0.02	38^{+27}_{-15}	8.5	1.00/479
M1	5.5 ± 0.4	0.61 ± 0.03	0.02	10	0.73 ± 0.03	0.17 ± 0.02	25^{+14}_{-12}	10.5	1.00/479
M2	1.2 ± 0.2	0.62 ± 0.03	12.5	0.37	0.72 ± 0.02	0.21 ± 0.02	44^{+24}_{-16}	7.7	1.02/479

^aBB: blackbody fit. F: N_{H} fixed to the Galactic value; M1: R^∞ fixed to the maximum value to meet the optical upper limit; M2: R^∞ fixed to the minimum value to meet the blackbody fit.

^bOptical depth at the absorption line center.

^cErrors not shown due to poor fit.

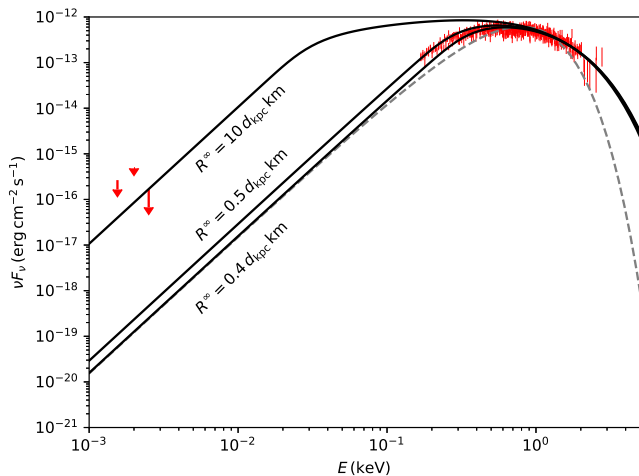


Figure 2. Combined data (red bars) and the fitting results. The red triangle and arrows are the optical flux upper-limit given by *Gemini-North* (Rutledge et al. 2008) and *GTC* (Shibanov et al. 2016). The gray dashed line is the one-component blackbody fitting. The solid lines are the best-fits for model F, M1 and M2. Galactic absorption is not shown.

4. TORQUED BY MAGNETOSPHERIC ACTIVITY?

In the vacuum gap model for radio emission of neutron stars, Ruderman & Sutherland (1975) propose the idea of death line, below which the electric potential of the gap region is too low ($< \Phi_c = 10^{12} \text{ V}$) to generate electron-positron pairs for curvature radiation. The maximum potential drop (Φ_m) above the surface of a neutron star is

$$\Phi_m = \frac{2\pi^2}{c^2 P^2} BR^3, \quad (3)$$

which yields the death line

$$R_{\text{max,km}}^3 = 1.52 \times 10^2 B_{12}^{-1} P_s^2, \quad (4)$$

on the premise that gap sparking could occur if $\Phi_m > 10^{12} \text{ V}$. Assuming that magnetic dipole radiation accounts for the spin-down, we plot the death lines on the $P - \dot{P}$ diagram (Figure 1) for typical neutron star radius $R = 10 \text{ km}$ (red dotted line) and smaller strangeon star radii (red solid lines). Note that strangeon star with smaller radius (i.e., smaller momentum inertia) would exhibit larger magnetic field than that indicated by the dashed lines in Figure 1. To meet the criterion that Calvera is dead, the upper limit for the stellar radius is 0.66 km , which yields a stellar mass $M = 3 \times 10^{-4} M_\odot$. Therefore, in the context of dead pulsar, Calvera can be interpreted as a low-mass strangeon star. However, these values are extreme even for strangeon stars. This problem could be alleviated if alternative mechanisms contribute to the spin-down. In our model (see Section 5), the X-ray emission is maintained by the accretion (with a rate $\dot{M}_X = 1.2 \times 10^{12} d_{\text{kpc}}^2 \text{ g s}^{-1}$ on to the surface) which could also provide a torquebraking the rapid-rotating low-mass star and accounting for the observed \dot{P} .

5. TORQUED BY FALL-BACK DISK?

The detailed mechanism of the accretion has significant impact on the long-term evolution and leads to distinct observational consequences. Two kinds of accretion source are discussed in literature.

Interstellar medium (ISM) accretion is first proposed by Ostriker et al. (1970) to understand the X-ray luminosity of INS (Treves & Colpi 1991; Blaes & Madau 1993, also see Treves et al. 2000 for reviews). In this scenario, old INS traveling slowly through dense

ISM accrete efficiently and exhibit less luminous ($\lesssim 10^{31} \text{ erg s}^{-1}$) thermal soft X-ray spectra. This model may explain the optical excess from the X-ray extrapolation (Zane et al. 2000) that is supported by succedent observations (e.g., Kaplan et al. 2011).

However, the relatively high proper motion and low ambient ISM density of XDINS cast doubts on the ISM accretion picture. Alternatively, it is reasonable that not all matter are expelled in the supernova explosion (Colgate 1971; Chevalier 1989) and a fractional infalling material may form a fall-back disk. The propeller or accretion torques of the disk can explain the high spin-down rate of neutron stars (Alpar 2001; Chatterjee et al. 2000; Ertan et al. 2009, 2014; Benli & Ertan 2016; Ertan et al. 2017) including XDINSs, the anomalous X-ray pulsars and soft gamma-ray repeaters (AXPs and SGRs, see Olausen & Kaspi 2014; Kaspi & Beloborodov 2017, for reviews), the latter are otherwise interpreted as magnetars (Thompson & Duncan 1995). Especially, in the picture of Alpar (2001), XDINSs, AXPs and SGRs which populate similar region in the $P - \dot{P}$ diagram can be unified by the asymptotic propeller/accretion mechanism with alternative pathways. In this scenario, the X-ray luminosity of AXP/SGR is caused by accretion (Benli & Ertan 2016) while that of XDINS is produced by energy dissipation in the neutron star (Alpar 2001, 2007) or by intrinsic cooling (Ertan et al. 2014), i.e., accretion onto the stellar surface is not necessarily assumed in the propeller phase. However, matter inflows are observed in simulations of ISM accretion propeller (Romanova et al. 2003) as well as disk accretion propeller (Romanova et al. 2017) and the portion of the accreting matter may be sufficient to maintain the SSA radiation.

Nevertheless, the NS-disk system is not expected to reside in vacuum. Therefore, we propose here that ISM regulates the debris/fall-back disk accretion as a supplement and can be the dominant accretion source in the late phase when the fall-back material depletes. In this *ISM-fed debris disk accretion* (IFDA) picture, we expect $\dot{M}_A > \dot{M}_X > \dot{M}_B$ when the fall-back system forms, where \dot{M}_B is the ISM accretion rate at the Bondi radius (Bondi 1952) and \dot{M}_A is the accretion rate at the Alfvén radius (Ghosh & Lamb 1979). Note that \dot{M}_A decreases as the disk loses its mass gradually through accretion and propeller wind. In the late phase of the evolution, the system will reach an equilibrium at $\dot{M}_X = \dot{M}_B < \dot{M}_A$ where the ISM accretion fully accounts for the NS luminosity. At this stage, a disk structure could remain but it would become thicker as it is fed by the ISM accretion and \dot{M}_A does not decrease over time. If the initial mass of the fall-back disk is small, the system could also evolve to the spherical ISM accretion regime.

We assume that the fall-back disk is formed, or main-

tained by the ISM, and is associated with Calvera. The accreted matter fall almost Keplerianly towards the Alfvén radius r_A (Ghosh & Lamb 1979)

$$r_A = \left(\frac{B^2 R^6}{\dot{M}_A \sqrt{2GM}} \right)^{2/7} = 6.18 \times 10^8 B_{12}^{4/7} R_{\text{km}}^{12/7} M_1^{-1/7} \dot{M}_{A,10}^{-2/7} \text{ cm}, \quad (5)$$

where B_{12} is the surface magnetic field in units of 10^{12} G, R_{km} the stellar radius in units of km, M_1 the stellar mass in units of M_\odot , $\dot{M}_{A,10}$ is the accretion rate at r_A in units of 10^{10} g s^{-1} . Matter accumulated at r_A will be forced to co-rotate with the NS and most of the mass would be expelled centrifugally due to the propeller effect (Illarionov & Sunyaev 1975). Consequently, the co-rotation and deflection of the matter would exert a negative torque N on the star which contributes to the spin-down of the pulsar (Liu et al. 2014),

$$N = 2\dot{M}_A r_A^2 \Omega_K(r_A) \left[1 - \left(\frac{\Omega}{\Omega_K(r_A)} \right)^\chi \right] = -I \frac{2\pi}{P^2} \dot{P}, \quad (6)$$

where $\Omega_K(r_A) = (GM/r_A^3)^{1/2}$ is the Keplerian angular velocity at r_A . The factor χ is introduced to account for the the inefficiency of the propeller effect ($0 < \chi < 1$). This formula reduces to the prevailing form when $\chi = 1$ (Menou et al. 1999; Chatterjee et al. 2000). We assume the momentum inertia of the star to be $I = MR^2/2$ and the mass-radius relation for a low-mass strangeon star can be approximated by $M = 4\pi\rho R^3/3$, where the density ρ is a few times the nuclear density ρ_n (Lai & Xu 2009; Lai et al. 2013; Guo et al. 2014). We fix $\rho = 2\rho_n$. Combining equation (5) and (6), we obtain

$$\dot{P} = 4.3 \times 10^{-12} B_{12}^{8/7} R_{\text{km}}^{-17/7} P_s \dot{M}_{A,10}^{3/7} \frac{\omega_s^\chi - 1}{\omega_s} \text{ s s}^{-1}, \quad (7)$$

where the fastness $\omega_s = \Omega/\Omega_K(r_A)$ and $\omega_s > 1$ in the propeller phase.

Most of the mass accreted to the the Alfvén radius are expelled and only a small portion of the matter are accumulated onto the strangeon star surface (Romanova et al. 2017), i.e., $\dot{M}_A = \eta \dot{M}_X$ with $\eta > 1$. \dot{M}_X can be inferred from the X-ray luminosity, $L_X = 4\pi d^2 F_X \approx 0.1 \dot{M}_X c^2$. We use the flux obtained by the spectral fit $F_{X,0.3-10 \text{ keV}} = 9.0 \times 10^{-13} \text{ erg cm}^{-2} \text{ s}^{-1}$ for calculation. The factor 0.1 is the approximate energy conversion efficiency which is dominated by the gravitational potential for massive star and by the strangeonization energy release for low-mass star.

We present the parameter space of B and R in Figure 3. The red curve is the upper limit of the stellar radius beyond which the surface electric potential would ex-

ceed Φ_c and the NS would be radio active (equation 4). Contours for ηd_{kpc}^2 are in solid black lines. According to the definition $\eta > 1$ and the speculation that Calvera can be as close as ~ 0.3 kpc (Halpern & Gotthelf 2015), $\eta d_{\text{kpc}}^2 = 0.1$ can be regarded as a lower limit which yields $B \lesssim 10^{11}$ G. The gray dashed lines are the contours of \dot{P}_{dip} and the shaded area on the right is prohibited. The blue dashed line is the $\omega_s = 1$ contour and the shaded area on the left is also banned since it contradicts with our accretion-spin-down model. The ratio of matter permeate through the Alfvén radius is confusing (Romanova et al. 2003, 2017) and therefore left the upper limit of ηd_{kpc}^2 highly uncertain. However, the intersection point of the blue line and the red line provides the upper limit of Calvera ($R \lesssim 4$ km, $M \lesssim 0.1 M_\odot$ for a efficient $\chi = 1$ propeller), which yields a negligible redshift factor $(1 - 2GM/c^2R)^{-1/2} \lesssim 1.1$. Most of the parameter space agree with a low magnetic field $B < 10^{11}$ G. The matter accreted to the polar cap diffuse across the star surface with a timescale $\tau \propto B^2$ (Wang et al. 2017b) and can cover the whole surface for a small B . Therefore, we assume $R = R^\infty$ in the following discussion.

Joining the parameters constrained by spectral modeling and the dead-pulsar criterion, we plot in Figure 4 the contours with respect to the stellar (radiation) radius R^∞ and the distance d . The upper/lower limits of the spectral normalization are plotted as black solid lines. The colorful lines within the permitted space represent different combinations of η and B and color-coded by B . The contour lines are cut off at the maximum radii (dashed lines) regarding to the value of B . The maximum radius is defined by both the death line criterion and the fastness criterion, therefore a lower magnetic field might corresponds to a smaller maximum radius (e.g, the upper panel of Figure 4, see Figure 3). The logarithm of η is tagged below each contour line. For larger B , i.e., with a smaller maximum radius, the contours of η begin at larger radii. Therefore, beyond a certain value of B , no reasonable η can satisfy the upper limit in the optical band. We use $\eta > 1$ and, again, conclude that $B \lesssim 10^{11}$ G.

According to the observed flux of Calvera, $\dot{M}_X = 1.2 \times 10^{12} d_{\text{kpc}}^2 \text{ g s}^{-1}$. For ISM accretion, the accretion rate at the Bondi radius (Bondi 1952) is

$$\dot{M}_B = 4\pi\rho_\infty \frac{(GM)^2}{v^3}, \quad (8)$$

where ρ_∞ is the ISM density, assumed to be $10^{-24} \rho_{24} \text{ g cm}^{-3}$, v the speed of the star which is inferred from the proper motion measurement to be $v_\perp = 286 \pm 110 d_{\text{kpc}} \text{ km s}^{-1}$ (Halpern & Gotthelf 2015). This

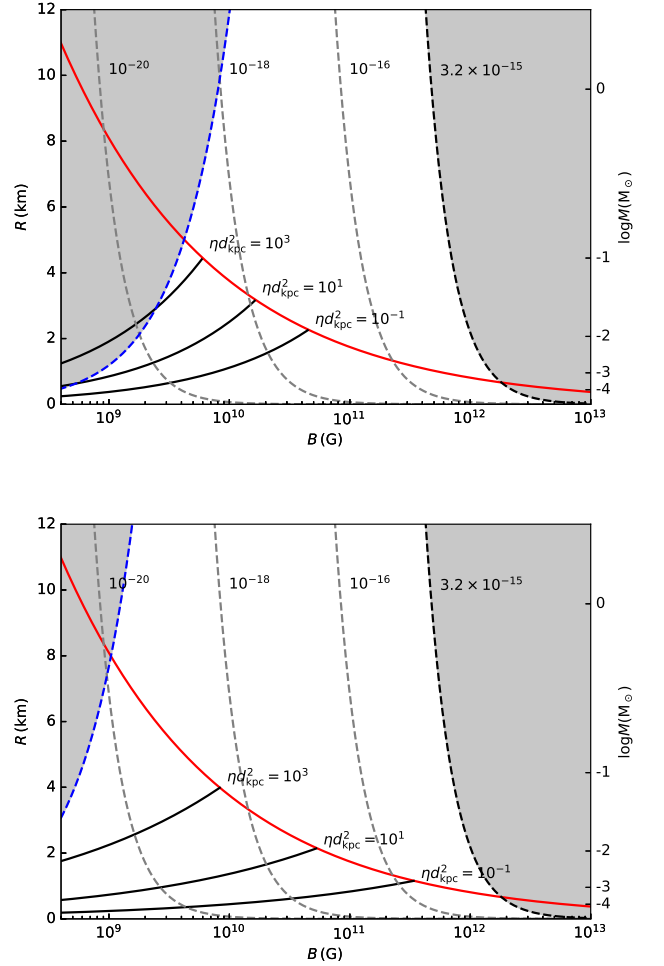


Figure 3. The parameter space of B and R for $\chi = 1$ (upper panel) and $\chi = 1/2$ (lower panel). The red solid curve shows the maximum permitted stellar radius of a dead strangeon star. Different choices of ηd_{kpc}^2 are plotted as black solid lines. The gray dashed lines are the contours for \dot{P}_{dip} and $\dot{P}_{\text{dip}} > 3.2 \times 10^{-15}$ is prohibited. The shaded area defined by the blue dashed line corresponds to $\omega_s < 1$ which contradicts to the propeller-torqued-spin-down model. For most of the permitted parameter space, Calvera experiences a low surface magnetic field.

results in $\dot{M}_B = 10^7 \rho_{24} M_1^2 d_{\text{kpc}}^{-3} \text{ g s}^{-1}$ and

$$\frac{\dot{M}_X}{\dot{M}_B} = 10^5 \rho_{24}^{-1} M_1^{-2} d_{\text{kpc}}^5. \quad (9)$$

Even for a very small d (e.g., 0.1 kpc), the matter accretes on the stellar surface faster than the Bondi accretion and $\dot{M}_A = \eta \dot{M}_X \approx 10^{11-15} \text{ g s}^{-1}$ is even higher. The latter rate is typical for a fall-back disk of 10^5 yr (Alpar et al. 2001; Ertan et al. 2009), indicating that Calvera is at the early phase of the IFDA evolution, which is often expected from a pulsar with small period.

We illustrate the evolution of Calvera in Figure 5, assuming $R = 2$ km and different B values. The decrease

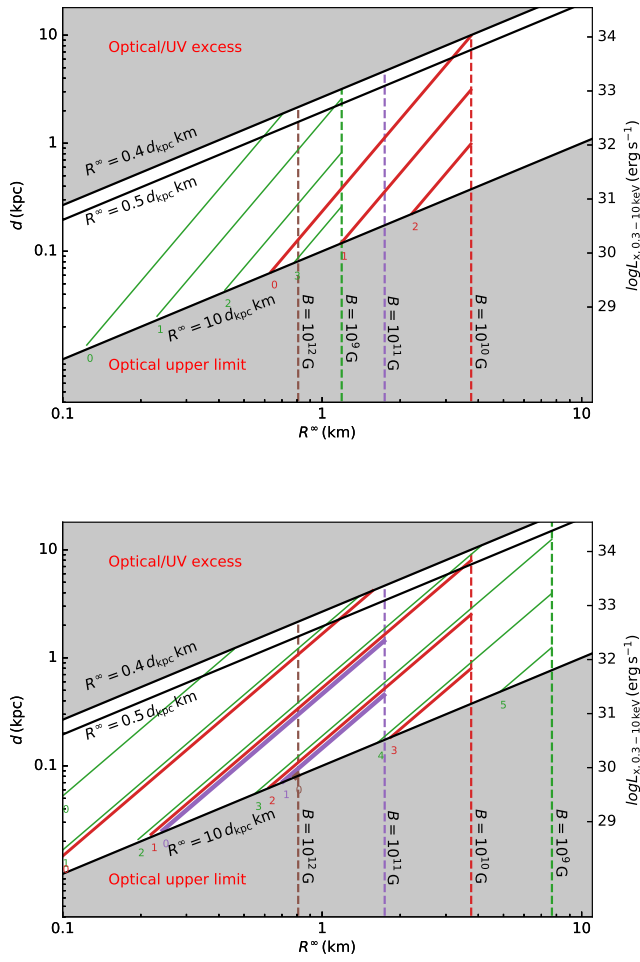


Figure 4. The parameter space of radiation radius (R^∞) and distance (d) for $\chi = 1$ (upper panel) and $\chi = 1/2$ (lower panel). Due to the low redshift factor and the low surface magnetic field, we assume R^∞/d from surface F, M1 and M2 are shown as black solid contour lines. The shaded spaces are prohibited due to the optical upper limit and optical/UV excess constraints. The colorful lines represent different combinations of B and η . Lines are color-coded (also with different line thickness) by B and the contours are cut off at the maximum radii (dashed lines) corresponding to B . The value of η ranges from $1 - 10^4$ and their logarithms are tagged below each line. We regard $\eta = 1$ as a lower bound, consequently, $B \gtrsim 10^{11}$ is unlikely since the parameter space is limited.

of the accretion rate of the fall-back disk is modeled by a power-law (Menou et al. 2001) $\dot{M}_A = \dot{M}_0(t/T)^{-\alpha}$ (red lines). We set $T = 1000$ s and the current age of Calvera to be the characteristic age 3.2×10^5 yr but the detailed values are not very important. $\alpha = 7/6$ is adopted from Liu et al. (2014) which is similar to that in Cannizzo et al. (1990).

Though unlikely to be the accretion source of Calvera, we note that the ISM accretion predicts a braking index $n = \dot{\Omega}/\dot{\Omega}^2 \approx \chi$ (assuming that the ISM feed the

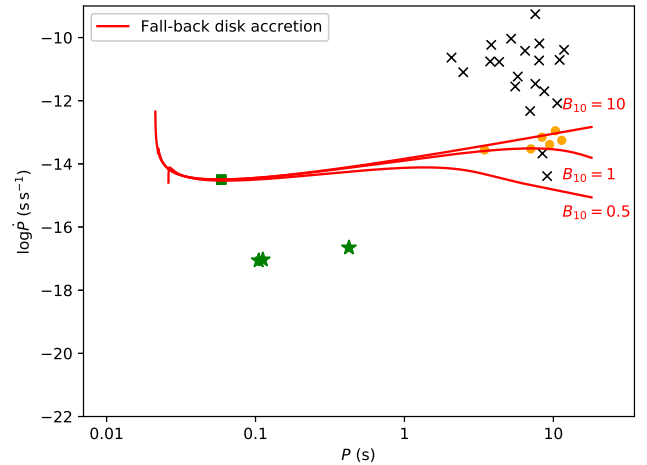


Figure 5. The evolution tracks of Calvera in the IFDA model (red), with an assumption of $\chi = 1$ and a stellar radius $R = 2$ km. Magnetic field $B = B_{10} \times 10^{10}$ G. Pulsar notations are same with those in Figure 1. We use $\dot{M}_A = \dot{M}_0(t/T)^{-\alpha}$ where the time scale $T = 1000$ s, $\alpha = 7/6$ and $\dot{M}_0 \sim 10^{21-25}$ g s $^{-1}$.

disk at a constant rate). The fall-back disk model, on the other hand, predicts an infinite large braking index in the early evolution (last for $\sim 10^2$ yr, unlikely to be observable) which falls to a value ~ 1 during the migration. It also shows that Calvera would eventually evolve to the XDINS region within 10^7 yr for $B_{10} = 10$, or 10^8 yr for $B_{10} = 0.5$, and populates in a clustered area despite different B values. Therefore, Calvera could be a progenitor of XDINS which is self-consistent since the radiation properties of the latter is also interpreted in the framework of the SSA model (Wang et al. 2017b). In this late phase, transition from the fall-back disk accretion to ISM accretion may occur (Wang et al. 2017a).

6. DISCUSSION

6.1. Distance

The distance of Calvera is highly uncertain due to the lack of radio observation and optical counterpart identification. Generally, the distance estimation can be obtained through three methods: (1) Luminosity; (2) N_H column; and (3) proper motion measurement. Unfortunately, the first two methods are spectral-model dependent and the luminosity is even less constrained in the SSA model due to the lack of optical data. For the lower limit of R^∞ in the *XMM-Newton* spectrum fit, we have a lower limit of $N_H = (1.3 \pm 0.2) \times 10^{20}$ cm $^{-2}$. This value is comparable to the galactic value 2.65×10^{20} cm $^{-2}$ (Kalberla et al. 2005), placing Calvera beyond the radius of the Local Bubble (Cox & Reynolds 1987). For a conservative estimation, we suggest $d > 100$ pc (Lallement et al. 2003; Miller & Bregman 2015;

Halpern & Gotthelf 2015) as the distance lower limit.

The model independent estimation comes from the proper motion measurement. Halpern & Gotthelf (2015) obtain the proper motion of Calvera to be $69 \pm 26 \text{ mas yr}^{-1}$ corresponding to a transverse velocity $v_{\perp} = 286 \pm 110 d_{\text{kpc}} \text{ km s}^{-1}$ with respect to the local standard of rest. Given the typical transverse velocity of XDINS to be $150 - 300 \text{ km s}^{-1}$ (e.g., Kaplan 2008) and its high Galactic latitude, it is not likely that Calvera is a far away pulsar and $d \lesssim 1 \text{ kpc}$ can be a hypothetical upper limit.

6.2. Calvera as a CCO

The connections between Calvera and the CCO have been hotly debated since its discovery. The non-detection of the supernova remnant (within 2° , Rutledge et al. 2008) places Calvera as a candidate of the first orphaned CCO. In this work, we provide more evidence for this argument.

The best-fit temperature of Calvera in the context of a neutron star atmosphere result in $\lesssim 0.2 \text{ keV}$ (Zane et al. 2011; Shibano et al. 2016)—smaller than that of known CCOs which are within the range $0.3 - 0.7 \text{ keV}$ (e.g., Hui & Becker 2006; Pavlov et al. 2001, 2000; Park et al. 2006, also see Figure 2 in Rutledge et al. 2008). This was then attributed to the intrinsic cooling, however, the temperature of Calvera in the SSA model $\approx 0.6 \text{ keV}$ readily fits in the CCO population.

The main counter-argument for Calvera being a CCO is its upper position in the $P - \dot{P}$ diagram (i.e., the high magnetic field). Ho (2011) propose that the magnetic field can be buried by prompt fall-back supernova ejecta and be recovered within 10^4 yr . In our accretion-braked dead strangeon star scenario, the magnetic field of Calvera is constrained at $B \lesssim 10^{11} \text{ G}$ by its flux upper limit in the optical band, which brings Calvera closer to the CCO family. In either picture, Calvera can be interpreted as a (orphaned) CCO. A discriminative probe would be the future measurement of the braking index. For an accretion braked pulsar, $n > 0$ in the early phase, whereas CCO with rapid field growth would exhibit a large negative braking index (Viganò & Pons 2012; Bernal et al. 2013). Unifying CCO and XDINS within the IFDA picture will be presented in a coming

paper.

7. SUMMARY

In the framework of the strangeon star model, we conclude that Calvera is a dead low-mass strangeon star ($\lesssim 0.1 M_{\odot}$) with a small radius ($\lesssim 4 \text{ km}$) and weak magnetic field ($\lesssim 10^{11} \text{ G}$) which is most likely braked by the fall-back disk accretion.

Nevertheless, a decisive judgment on the nature of Calvera will only come from future observations. The optical flux measurement will be crucial in determining the $d - R^{\infty}$ relation (Figure 4). In our optical/UV excess picture, we predict the lower limit of the optical magnitude to be $g' \lesssim 35$ which is challenging even for future instruments (e.g., Thirty Meter Telescope (TMT), Nelson & Sanders 2008). However, it is possible that the optical flux is higher than the lower limit by a factor of $5 - 12$ (Kaplan et al. 2011), making it more accessible. Future timing analysis can distinguish the braking mechanisms (either by accretion or by magnetic dipole radiation or by rapid magnetic field growth). The long-term timing monitoring can be achieved with the enhanced X-ray Timing and Polarimetry (eXTP, Zhang et al. 2016); the Neutron star Interior Composition Explorer (NICER, Gendreau et al. 2012); the Advanced Telescope for High-ENergy Astrophysics (Athena, Barret et al. 2016) and the Lynx mission (Gaskin et al. 2015). If Calvera is indeed a near pulsar, a distance measurement will also benefit from the future deep optical observation or soft X-ray timing. Although not possible at present (Zane et al. 2011), future detection of radio and gamma-ray emission will differentiate whether Calvera is a dead pulsar.

We thank Dr. Andrey Danilenko for drawing our attention to the interesting object, Calvera, during his visiting KIAA. We are grateful to all members in the pulsar group at Peking University and Dr. Xiangdong Li at Nanjing University for discussions. This work is supported by the National Natural Science Foundation of China (no. 11673002 and U1531243) and the Strategic Priority Research Program of CAS (no. XDB23010200).

Software: Xspec (Arnaud 1996), CIAO (Fruscione et al. 2006), SAS (SAS development Team 2014)

REFERENCES

- Alpar, M. A. 2001, ApJ, 554, 1245
 —. 2007, Ap&SS, 308, 133
 Alpar, M. A., Ankay, A., & Yazgan, E. 2001, ApJL, 557, L61
 Arnaud, K. A. 1996, in PASP, Vol. 101, Astronomical Data Analysis Software and Systems V, ed. G. H. Jacoby & J. Barnes, 17
 Barret, D., Lam Trong, T., den Herder, J.-W., et al. 2016, in Proc. SPIE, Vol. 9905, Space Telescopes and Instrumentation 2016: Ultraviolet to Gamma Ray, 99052F
 Benli, O., & Ertan, Ü. 2016, MNRAS, 457, 4114
 Bernal, C. G., Page, D., & Lee, W. H. 2013, ApJ, 770, 106

- Bhattacharya, D., Wijers, R. A. M. J., Hartman, J. W., & Verbunt, F. 1992, *A&A*, 254, 198
- Blaes, O., & Madau, P. 1993, *ApJ*, 403, 690
- Bondi, H. 1952, *MNRAS*, 112, 195
- Cannizzo, J. K., Lee, H. M., & Goodman, J. 1990, *ApJ*, 351, 38
- Chatterjee, P., Hernquist, L., & Narayan, R. 2000, *ApJ*, 534, 373
- Chevalier, R. A. 1989, *ApJ*, 346, 847
- Colgate, S. A. 1971, *ApJ*, 163, 221
- Cox, D. P., & Reynolds, R. J. 1987, *ARA&A*, 25, 303
- Ertan, Ü., Çalıřkan, ř., Benli, O., & Alpar, M. A. 2014, *MNRAS*, 444, 1559
- Ertan, Ü., alıřkan, ř., & Alpar, M. A. 2017, *MNRAS*, 470, 1253
- Ertan, Ü., Ekři, K. Y., Erkut, M. H., & Alpar, M. A. 2009, *ApJ*, 702, 1309
- Fruscione, A., McDowell, J. C., Allen, G. E., et al. 2006, in *Proc. SPIE*, Vol. 6270, Society of Photo-Optical Instrumentation Engineers (SPIE) Conference Series, 62701V
- Gaskin, J. A., Weisskopf, M. C., Vikhlinin, A., et al. 2015, in *Proc. SPIE*, Vol. 9601, UV, X-Ray, and Gamma-Ray Space Instrumentation for Astronomy XIX, 96010J
- Gendreau, K. C., Arzoumanian, Z., & Okajima, T. 2012, in *Proc. SPIE*, Vol. 8443, Space Telescopes and Instrumentation 2012: Ultraviolet to Gamma Ray, 844313
- Ghosh, P., & Lamb, F. K. 1979, *ApJ*, 234, 296
- Gotthelf, E. V., Halpern, J. P., & Alford, J. 2013, *ApJ*, 765, 58
- Guo, Y., Lai, X., & Xu, R. 2014, *ChPhC*, 38, 055101
- Haberl, F. 2007, *Ap&SS*, 308, 181
- Halpern, J. P. 2011, *ApJL*, 736, L3
- Halpern, J. P., Bogdanov, S., & Gotthelf, E. V. 2013, *ApJ*, 778, 120
- Halpern, J. P., & Gotthelf, E. V. 2010, *ApJ*, 709, 436
- . 2015, *ApJ*, 812, 61
- Hessels, J. W. T., Stappers, B. W., Rutledge, R. E., Fox, D. B., & Shevchuk, A. H. 2007, *A&A*, 476, 331
- Ho, W. C. G. 2011, *MNRAS*, 414, 2567
- Hui, C. Y., & Becker, W. 2006, *A&A*, 454, 543
- Illarionov, A. F., & Sunyaev, R. A. 1975, *A&A*, 39, 185
- Kalberla, P. M. W., Burton, W. B., Hartmann, D., et al. 2005, *A&A*, 440, 775
- Kaplan, D. L. 2008, in *American Institute of Physics Conference Series*, Vol. 983, 40 Years of Pulsars: Millisecond Pulsars, Magnetars and More, ed. C. Bassa, Z. Wang, A. Cumming, & V. M. Kaspi, 331–339
- Kaplan, D. L., Kamble, A., van Kerkwijk, M. H., & Ho, W. C. G. 2011, *ApJ*, 736, 117
- Kaspi, V. M., & Beloborodov, A. M. 2017, *ARA&A*, 55, 261
- Lai, X. Y., Gao, C. Y., & Xu, R. X. 2013, *MNRAS*, 431, 3282
- Lai, X. Y., & Xu, R. X. 2009, *MNRAS*, 398, L31
- Lai, X.-Y., & Xu, R.-X. 2011, *Research in Astronomy and Astrophysics*, 11, 687
- Lai, X.-Y., & Xu, R.-X. 2017, in *Journal of Physics Conference Series*, Vol. 861, *Journal of Physics Conference Series*, 012027
- Lallement, R., Welsh, B. Y., Vergely, J. L., Crifo, F., & Sfeir, D. 2003, *A&A*, 411, 447
- Li, Z., Qu, Z., Chen, L., et al. 2015, *ApJ*, 798, 56
- Liu, X.-W., Xu, R.-X., Qiao, G.-J., Han, J.-L., & Tong, H. 2014, *Research in Astronomy and Astrophysics*, 14, 85
- Manchester, R. N., Hobbs, G. B., Teoh, A., & Hobbs, M. 2005, *AJ*, 129, 1993
- Menou, K., Esin, A. A., Narayan, R., et al. 1999, *ApJ*, 520, 276
- Menou, K., Perna, R., & Hernquist, L. 2001, *ApJL*, 554, L63
- Miller, M. J., & Bregman, J. N. 2015, *ApJ*, 800, 14
- Nelson, J., & Sanders, G. H. 2008, in *Proc. SPIE*, Vol. 7012, *Ground-based and Airborne Telescopes II*, 70121A
- Olausen, S. A., & Kaspi, V. M. 2014, *ApJS*, 212, 6
- Ostriker, J. P., Rees, M. J., & Silk, J. 1970, *Astrophys. Lett.*, 6, 179
- Park, S., Mori, K., Kargaltsev, O., et al. 2006, *ApJL*, 653, L37
- Pavlov, G. G., Sanwal, D., Kızıltan, B., & Garmire, G. P. 2001, *ApJL*, 559, L131
- Pavlov, G. G., Zavlin, V. E., Aschenbach, B., Trümper, J., & Sanwal, D. 2000, *ApJL*, 531, L53
- Romanova, M. M., Blinova, A. A., Ustyugova, G. V., Koldoba, A. V., & Lovelace, R. V. E. 2017, *arXiv:1704.08336*
- Romanova, M. M., Toropina, O. D., Toropin, Y. M., & Lovelace, R. V. E. 2003, *ApJ*, 588, 400
- Ruderman, M. A., & Sutherland, P. G. 1975, *ApJ*, 196, 51
- Rutledge, R. E., Fox, D. B., & Shevchuk, A. H. 2008, *ApJ*, 672, 1137
- SAS development Team. 2014, *SAS: Science Analysis System for XMM-Newton observatory*, *Astrophysics Source Code Library*, , ascl:1404.004
- Shevchuk, A. S. H., Fox, D. B., & Rutledge, R. E. 2009, *ApJ*, 705, 391
- Shibanov, Y., Danilenko, A., Zharikov, S., Shternin, P., & Zyuzin, D. 2016, *ApJ*, 831, 112
- Thompson, C., & Duncan, R. C. 1995, *MNRAS*, 275, 255
- Treves, A., & Colpi, M. 1991, *A&A*, 241, 107
- Treves, A., Turolla, R., Zane, S., & Colpi, M. 2000, *PASP*, 112, 297
- Turner, M. J. L., Abbey, A., Arnaud, M., et al. 2001, *A&A*, 365, L27
- van den Heuvel, E. P. J. 1987, in *IAU Symposium*, Vol. 125, *The Origin and Evolution of Neutron Stars*, ed. D. J. Helfand & J.-H. Huang, 393–404
- van Kerkwijk, M. H., & Kulkarni, S. R. 2001, *A&A*, 378, 986
- Viganò, D., & Pons, J. A. 2012, *MNRAS*, 425, 2487
- Voges, W., Aschenbach, B., Boller, T., et al. 1999, *A&A*, 349, 389
- Walter, F. M., & Matthews, L. D. 1997, *Nature*, 389, 358
- Wang, W., Feng, Y., Lai, X., et al. 2017a, *arXiv:1705.03763*
- Wang, W., Lu, J., Tong, H., et al. 2017b, *ApJ*, 837, 81
- Xu, R. X. 2003, *ApJL*, 596, L59
- Xu, R. X., Bastrukov, S. I., Weber, F., Yu, J. W., & Molodtsova, I. V. 2012, *PhRvD*, 85, 023008
- Zane, S., Turolla, R., & Treves, A. 2000, *ApJ*, 537, 387
- Zane, S., Haberl, F., Israel, G. L., et al. 2011, *MNRAS*, 410, 2428
- Zhang, S. N., Feroci, M., Santangelo, A., et al. 2016, in *Proc. SPIE*, Vol. 9905, *Space Telescopes and Instrumentation 2016: Ultraviolet to Gamma Ray*, 99051Q
- Zhou, E. P., Lu, J. G., Tong, H., & Xu, R. X. 2014, *MNRAS*, 443, 2705